

Internal Motions of Linear Chains and Spherical Microgels in Θ and Poor Solvents

Zhuojun Dai[†] and Chi Wu^{*,†,‡}

[†]*Department of Chemistry, The Chinese University of Hong Kong, Shatin, N.T., Hong Kong, and*

[‡]*The Hefei National Laboratory of Physical Science at Microscale, Department of Chemical Physics, The University of Science and Technology of China, Hefei, Anhui 230026, China*

Received August 4, 2010; Revised Manuscript Received October 12, 2010

ABSTRACT: Internal motions of narrowly poly(*N*-isopropylacrylamide) (PNIPAM) linear chains and spherical microgels in a very dilute aqueous solution and dispersion were studied under the Θ and poor solvent conditions by dynamic laser light scattering (LLS) over a wide range of scattering angles. As expected, only one narrow peak related to the translational diffusion was observed in the line-width distribution $G(\Gamma)$ of both linear chains and spherical microgels when $x < 1$, where $x = (qR_g)^2$ with q and R_g the scattering vector and the radius of gyration, respectively. As x increases to approach 1, we start to see a second peak related to fast internal motions of linear chains, whose average line width is related to some of the internal motions (normal modes) predicted in the nondraining bead-and-spring model. However, for swollen microgels, the second peak related to the internal motions only appears when x is much higher ($1/q \sim 50$ nm), indicating that thermal energy is not able to excite the entire microgel but only a small portion of the gel network. As the solvent quality changes from good to poor, the shrinking of a linear chain or subchains in the gel network gradually suppresses the internal motions, presumably due to stronger intersegment interaction. Surprisingly, we found that the relative contribution of the second peak makes a turning near the Θ temperature, leading to a new way to estimate the Θ condition of a given polymer solution.

Introduction

As a fundamental problem in polymer physics, the dynamics of flexible polymer chains in dilute solution has been intensely studied for years.^{1–6} When a polymer chain is sufficiently flexible (“soft”) to experience a large-scale configuration change, thermal motions of the chain segments will drive its configuration toward the most probable distribution. Such an intramolecular relaxation is named internal motion, as contrasted with the diffusive relaxation of its gravity center, which is also agitated by thermal energy.

In both the free-draining and the nondraining models, internal motions of a polymer chain is resolved into a series of normal modes with different frequencies. These internal motions together with the translational diffusion contribute to the spectrum of the scattered light. Their amplitudes have been theoretically evaluated on the basis of dynamical models with and without considering the hydrodynamic interaction. To study such a spectrum, dynamic laser light scattering (LLS) is a powerful technique to detect not only the translational diffusion of the center of mass of individual polymer chains in solution but also their internal dynamics, provided that their average radius of gyration (R_g) is comparable or larger than the reciprocal of the scattering vector (q) or in other words, is not much smaller than the wavelength of the laser light used, where $R_g = \langle R_g^2 \rangle_z^{1/2}$ is the root-mean square z -average radius of gyration, $q = (4\pi n/\lambda_0) \sin(\theta/2)$ is the scattering vector with n , λ_0 , and θ is the solvent refractive index, the wavelength in vacuum and scattering angle, respectively.

The Rouse-Zimm model was previously introduced to the dynamic LLS analysis by Pecora,³ deGennes,⁴ and Dubois-Violette⁷ on the basis of the concept of dynamic structure factor $S(q, t)$. When $qR_g \ll 1$, the relaxation induced by the translational

diffusion dominates $S(q, t)$. Therefore, $S(q, t)$ takes a form of single exponential decay if polymer chains are monodisperse. On the other hand, when $qR_g > 1$, $S(q, t)$ becomes a sum of multi-exponential terms due to the contributions from the internal motions.^{8–10} A combination of the line-width distributions $G(\Gamma)$ of narrowly distributed flexible long polymer chains, respectively, measured at a small and a high angle allows us to experimentally separate the translational and internal motions.¹¹

More quantitatively, when a coherent and monochromatic laser beam hits a dilute solution of linear flexible polymer chains without any adsorption, the scattered light has a spectral distribution, $S(q, \omega)$, due to the translational diffusion and internal motions as follows.¹²

$$S(q, \omega) = (1/2\pi) \int e^{-i\omega t} e^{-q^2 D|t|} S(q, t) dt \quad (1)$$

where ω is the angular frequency difference between the scattered and the incident light; D is the translational diffusion coefficient of individual chains; and $S(q, t)$ is generally expressed as

$$S(q, t) = \langle (1/N^2) \sum_{l=0}^N \sum_{m=0}^N e^{-iq \cdot [\mathbf{r}_l(0) - \mathbf{r}_m(t)]} \rangle \quad (2)$$

which is due to the interference of the scattered light from different segments within a long polymer chain made of N such segments, where $\mathbf{r}_l(0)$ is the position of the l th segment at time 0 and $\mathbf{r}_m(t)$ is the position of the m th segment at time t . The reference point is the center of mass of the chain. Therefore, all the spatial and temporal information related to intrachain, or called internal motions, is incorporated. Note that in a sufficiently diluted polymer solution, we can practically ignore the interchain interference. Using the Oseen–Kirkwood–Riseman hydrodynamic interaction and the

*The Hong Kong address should be used for all correspondences.

bead-and-spring model for a linear flexible polymer chain, the ensemble average in $S(q, \omega)$ is formulated as,¹³

$$\begin{aligned}
 S(q, \omega) = & P_0(x)L(\omega, q^2D) + \sum_{\alpha=1}^N P_1(x, \alpha)L(\omega, q^2D + \Gamma_\alpha) \\
 & + \sum_{\alpha=1}^N \sum_{\beta=1}^N P_2(x, \alpha, \beta)L(\omega, q^2D + \Gamma_\alpha + \Gamma_\beta) \\
 & + \sum_{\alpha=1}^N \sum_{\beta=1}^N \sum_{\gamma=1}^N P_3(x, \alpha, \beta, \gamma)L(\omega, q^2D + \Gamma_\alpha + \Gamma_\beta + \Gamma_\gamma) + \dots
 \end{aligned} \quad (3)$$

where $L(\omega, \Gamma)$ is a ω -normalized Lorentzian distribution, centered at the frequency (ω_0) of the incident light, with Γ the line-width at the half-height; and P_n ($n = 0, 1, \dots$), the contribution of each Lorentzian to the line-width distribution $G(\Gamma)$. $P_0(x)$, the zeroth-order contribution, is related to the translational diffusion; $P_1(x, \alpha)$, the first-order contribution of the α th internal mode; $P_2(x, \alpha, \beta)$, the second-order contribution of the α th and β th internal modes; and so on. At a sufficiently low scattering angle, i.e., $x \ll 1$, the observation length ($1/q$) is much larger than the chain size so that each chain can be viewed as a point without any internal structure; namely, P_n ($n \geq 1$) diminishes and $S(q, \omega)$ only contains the first term. As x increases, $1/q$ gradually decreases so that the light begins to probe a portion of the chain, P_n ($n \geq 1$) starts to contribute to $S(q, \omega)$ and the higher-order terms become more and more important. It has been numerically shown that $P_2(x, 1, 1)$ contributes the most to $S(q, \omega)$ among all the Lorentzian terms related to the internal motions.¹³

Nowadays, we normally directly measure the intensity–intensity time correlation function $G^{(2)}(q, t)$ of the scattered light in self-beating mode in real time in a modern LLS spectrometer, which can further lead to the dynamic structural factor $S(q, t)$, the Fourier transform of $S(q, \omega)$. Note that the highest reachable scattering angle in LLS spectrometers is practically limited to 160°. In previous research, experimental data has been accumulated mainly for polystyrene (PS), which has long been regarded as the best model polymer of linear flexible chains in both good and Θ solvents.^{14–19} The first cumulant $[\Omega(q)]$ obtained from the measured time correlation functions was found to be q^2 - and q^3 -dependent, respectively, for $qR_g \ll 1$ and $qR_g > 1$, which is in agreement with what is described in a non-free-draining model. At the same time, the characteristic relaxation time of the first and second modes, the plateau value of the reduced first cumulant, was measured for different PS solutions. Some of these experimental results are different from previous theoretical predictions, which are understandable because the theoretical model is oversimplified. The discrepancy led to a revision of classical theory and the birth of some new models.^{20,21}

In particular, we should mention a previous comparative study of the internal motions of poly(*N*-isopropylacrylamide) (PNIPAM) linear chains and spherical microgels under a good solvent condition.²² Note that PNIPAM is an extensively studied thermally sensitive polymer and individual linear PNIPAM chains free in a dilute solution or subchains in a PNIPAM gel network can undergo a coil-to-globule transition around 32 °C.^{23,24} Such a transition leads to the so-called volume “phase” transition, or more precisely, a sharp volume decrease (shrink) of a swollen gel network as the solution temperature increases across ~31–33 °C at which the solvent quality of water changes from good to poor. In the current study, we focused on the internal motions of narrowly distributed PNIPAM linear chains and spherical microgels during such a coil-to-globule transition. The objectives are (1) to find how the

internal motions are suppressed when the chain or subchains are shrinking and (2) to find any difference between individual linear chains and a gel network.

Experimental Section

Sample Preparation. The high molar mass poly(*N*-isopropylacrylamide) (PNIPAM) linear chains were made by a fractionation/filtration method.²⁵ The monodisperse PNIPAM microgel particles were synthesized by emulsion polymerization. The synthesis details can be found elsewhere.²⁶ Both PNIPAM linear chains ($M_w = 2.6 \times 10^7$ g/mol) and spherical microgels ($M_w = 3.4 \times 10^8$ g/mol) are narrowly distributed with a polydispersity index of 1.04 and 1.02, respectively. Each solution/dispersion was clarified by a filter (0.45 μ m; Millipore).

Laser Light Scattering (LLS). A modified commercial LLS spectrometer (ALV/DLS/SLS- 5022F) equipped with a multi- τ digital time correlator (ALV5000) and a cylindrical 22 mW UNIPHASE He–Ne laser ($\lambda_0 = 632$ nm) was used. The incident beam was vertically polarized with respect to the scattering plane. The details of the LLS instrumentation and theory can be found elsewhere.²⁷ Briefly, in static LLS, the excess absolute time-averaged scattered light intensity, known as the excess Rayleigh ratio $R_{rv}(\theta)$, at a given polymer concentration (C) and a given scattering angle (θ) is related to the weight-average molar mass (M_w), the square average radius of gyration ($\langle R_g^2 \rangle$), and the second virial coefficient (A_2) as

$$\left[\frac{KC}{R_{rv}(\theta)} \right] \approx \frac{1}{M_w} \left(1 + \frac{1}{3} \langle R_g^2 \rangle q^2 \right) + 2A_2C \quad (4)$$

where $K = 4\pi^2 n^2 (dn/dC)^2 / (N_A \lambda_0^4)$ with N_A and dn/dC , the Avogadro number and the specific refractive index increment, respectively. For PNIPAM in water at 25 °C, $dn/dC = 0.147$ mL/g.

In dynamic LLS, each measured $G^{(2)}(q, t)$ is related to the normalized electric field–field time correlation function $g^{(1)}(q, t)$ by $G^{(2)}(q, t) = A[1 + b|g^{(1)}(q, t)|^2]$, where A is a baseline; $0 \leq b \leq 1$, a spatial coherent constant depending on the instrumental detection optics. The value of b actually reflects the signal-to-noise ratio of a dynamic light-scattering experiment. It has been shown that $|g^{(1)}(q, t)|$ is proportional to $S(q, t)$ and related to the characteristic line-width distribution $G(\Gamma)$ by²⁸

$$g^{(1)}(q, t) = \int_0^\infty G(\Gamma) e^{-\Gamma t} d\Gamma \quad (5)$$

The Laplace inversion of each measured $g^{(1)}(q, t)$ leads to one $G(\Gamma)$ on the basis of eq 5. In this study, the CONTIN algorithm in the digital time correlator was used,²⁹ in which a probability factor of 50% was applied to regularize all of our fitting and the zero-order regularization was enforced to minimum the peak area under the line-width distribution. For a pure diffusive relaxation, such as for narrowly distributed polymer chains or spherical colloidal particles in a dilute solution or dispersion at $x \ll 1$, $G(\Gamma)$ can be converted into a translational diffusion coefficient distribution $G(D)$ by $D = \Gamma/q^2$ or further to a hydrodynamic radius distribution $f(R_h)$ by using the Stokes–Einstein equation.³⁰ As the scattering angle increases, $1/q$ becomes comparable to the size of a flexible and soft scattering object so that one has to consider the internal motions because their contributions to $G(\Gamma)$ become more and more important.

Results and Discussion

Figure 1 shows that the extrapolation of the time-average scattered light intensity at different solution temperatures to the zero angle leads to an identical value; i.e., there is no change in the weight-average molar mass, but the scattered light intensity becomes much less dependent on the scattering angle as the solution temperature increases. On the basis of eq 4, Figure 1

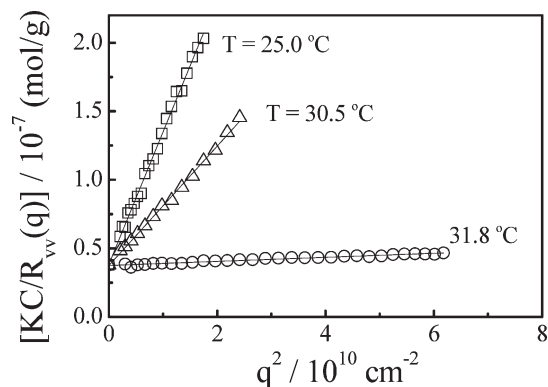


Figure 1. Scattering-vector (angular) dependent time-average scattered light intensity (Rayleigh ratio) of poly(*N*-isopropylacrylamide) linear chains in water at three different temperatures.

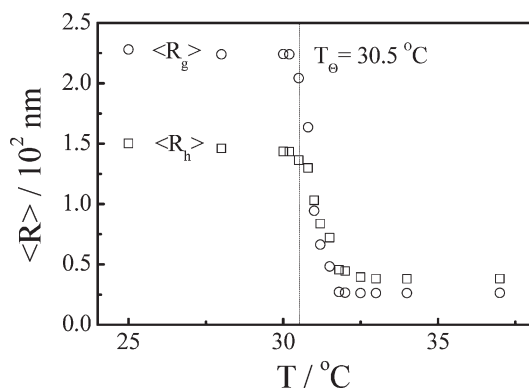


Figure 2. Solution-temperature dependent average radius of gyration and hydrodynamic radius of poly(*N*-isopropylacrylamide) linear chains in water.

clearly reveals the collapse of individual chains as the solution temperature increases with no interchain association. Otherwise, we would see an increase of the scattered light intensity at $q = 0$ because the scattered light intensity is proportional to the square of the mass of a scattering object. Figure 1 lays a solid ground for us to study internal motions of individual chains at different solution temperatures, especially under the Θ and poor solvent conditions. It should be noted that on the basis of eq 4, for a given temperature, the scattering intensity decreases as the scattering angle increases; while for a given scattering angle, the scattering intensity increases as the temperature increases (the chain shrinks), as shown in the Supporting Information (Figures 1s and 2s).

Figure 2 summarizes how the average sizes of individual polymer chains vary with the solution temperature, where the dash line marks the Θ temperature and the poor solvent region is on its right side. A comparison of the chain sizes under the good (lower temperatures) and the poor (higher temperatures) solvent conditions reveals that individual chains do not shrink too much up to the Θ temperature and the collapse of individual PNIPAM chains occur within a very narrow temperature window after passing the Θ point. Figure 2 enables us to calculate our experimentally reachable range of $x = (qR_g)^2$ at each solution temperature.

Figure 3 shows how the internal motions vary with the relative observation length scale (x) at 31.0 °C at which the chains are not fully collapsed yet, where the line-width (Γ) is scaled with both the translational diffusion coefficient (D) and scattering vector (q) so that the relaxation (line-width) related to the translational diffusion becomes unity. It is worth-noting that here $1/q$ is compared with R_g . For $x < 1$, i.e., $1/q > R_g$, each chain behaves just like a structure-less point so that we only see one peak with no

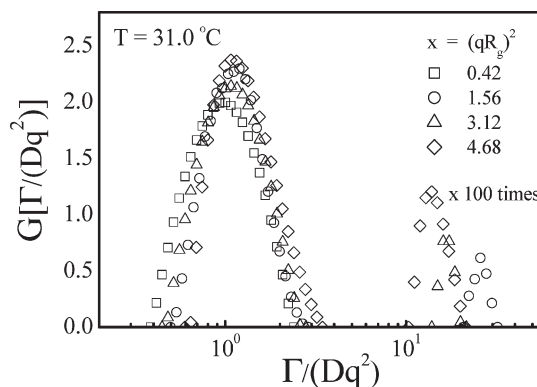


Figure 3. x -dependent Dq^2 -scaled line-width distributions $G[\Gamma/(Dq^2)]$ of poly(*N*-isopropylacrylamide) linear chains in water, where the peak related to internal motions is enlarged by a factor of 100 times for a better view.

interference from the internal motions. When $x \geq 1$, a second peak related to the internal motions appears in the measured line-width distribution, which relaxes 10–20 times faster than the translational diffusion.

An attentive reader might notice that the average position of the internal motions moves to the left (slow down) as x increases. The existing theories state that at $x > 1$, $S(q, t)$ of a flexible chain under both the free-draining³² and nondraining¹³ limit is dominated by the first five relaxation processes; namely, pure translational diffusion plus four principle internal motions. At $x > 1$, eq 3 in the time domain can be rewritten as

$$S(q, t) = \sum_{n=0}^{\infty} P_n e^{-\Gamma_n t} \quad (6)$$

The numerical values of P_n in the range $1 \leq x \leq 10$ have been calculated.¹³ Using the Zimm model,² we have

$$\Gamma_n = \frac{0.293RT\lambda'_n}{\eta_0 M[\eta]}$$

where $[\eta]$ and λ'_n are the intrinsic viscosity and the eigenvalues, respectively.³³ Normalized by Dq^2 and converting q to x , we can rewrite it as

$$\Gamma_n/(Dq^2) = \frac{0.293\lambda'_n R_g^2 RT}{xM[\eta]D\eta_0} \quad (7)$$

In the Stokes–Einstein equation, $RT/(D\eta_0) = 6\pi R_h N_A$. Therefore, eq 7 can further rewritten as

$$\Gamma_n/(Dq^2) = \frac{5.52\lambda'_n R_g^2 R_h}{xM[\eta]} = \frac{5.52\lambda'_n (R_g/R_h)^2 R_h^3}{xM[\eta]} \quad (8)$$

where R_g/R_h measures the chain conformation; and $M[\eta]$ is proportional to the hydrodynamic volume of a flexible chain and widely used in GPC for the universal calibration. Therefore, both R_g/R_h and $R_h^3/(M[\eta])$ are constants, independent of polymer and solvent for a given solution condition. Equation 8 reveals that $\Gamma_n/(Dq^2)$ decreases as x increases for a given solution temperature, which explains the shift of the average position of the second peak.

Figure 4 shows how the Dq^2 -scaled line-width distribution changes with the solution temperature for a given scattering angle. Note that here it is the change of $\langle R_g \rangle$ that varies x ; and $1/q \sim 54$ nm. The peak related to the internal motions becomes smaller and smaller as the solution temperature increases. Also

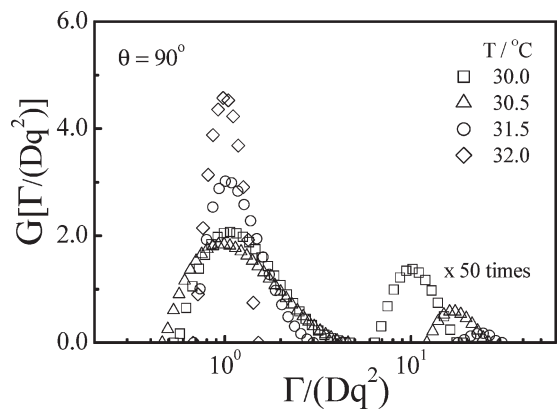


Figure 4. Solution-temperature dependent line-width distributions $G[\Gamma/(Dq^2)]$ of poly(*N*-isopropylacrylamide) linear chains in water, where the peak related to internal motions is enlarged by a factor of 50 times for a better view.

note that as the solution temperature increases beyond the Θ temperature (~ 30.5 °C), each chain in water dramatically shrinks and x decreases from 21.5 to 0.37 within the range 30.5–33.0 °C. In their fully collapsed state ($T \sim 33.0$ °C, $\langle R_g \rangle \sim 27$ nm and $x < 1$), there is only one diffusive relation and no internal motions appear. Equation 8 shows that for a given q , $\Gamma_n/(Dq^2)$ is proportional to $1/R_h^2$ because $R_h^3/(M[\eta]) = 9.56 \times 10^{-26}$ and 6.94×10^{-25} for a coiled chain and a hard sphere, respectively, which is a weak function of the chain conformation. This is why the peak related to internal motions in Figure 4 shifts to the right. On the other hand, the decrease of the peak area (the contribution of the internal motions to the line-width distribution) reflects the suppression of internal motions as each chain shrinks. To our knowledge, there has been no theory about such a decrease yet, but it is physically reasonable; namely, as the chain collapses, it becomes more and more difficult for the thermal energy ($k_B T$) to excite its internal motions.

Figure 5 shows that the average chain density increases from 3×10^{-3} to 1.9×10^{-1} g/cm³ as individual PNIPAM chains collapse from a random-coil to a uniform globule conformation, where $\langle \rho \rangle_{\text{chain}}$ is defined as $M_w/(4N_A\pi\langle R_h \rangle^3/3)$. Note that even in its fully collapsed state, each chain, on average, still contains about 80% of water inside its hydrodynamic volume, not as dry as we normally thought. On the other hand, we can further calculate the temperature and angular dependence of the relative intensity-weighting of the internal motions [$A_I/(A_I + A_D)$] from the area ratio of the two peaks in Figures 3 and 4, as shown in Figure 6.

In the good solvent region, $A_I/(A_I + A_D)$ essentially remains a constant for each given scattering angle, revealing that the slight shrinking of individual chains in this region has no effect on its internal motions because each chain still remains a random-coil conformation. When the solvent quality becomes poorer, $A_I/(A_I + A_D)$ dramatically drops and the internal motions disappear at temperatures higher than ~ 32 °C at which the chain is collapsed. Surprisingly, at different scattering angles, $A_I/(A_I + A_D)$ always turns near the Θ temperature. Again, there is no theory to predict such a turning point, but it is physically reasonable. Namely, polymer chains are agitated by the thermal energy, to undergo the internal motions they have to overcome the entropic force in a good solvent because of the chain swelling and the segment–segment interaction (enthalpy) in a poor solvent. At its “ideal” state, the entropic cost is balanced by the enthalpy interaction.

Figure 7 shows a combination of results in Figures 5 and 6; namely, how $A_I/(A_I + A_D)$ decreases while individual chain undergoes the coil-to-globule transition to increase the average chain density at different scattering angles. For each given chain

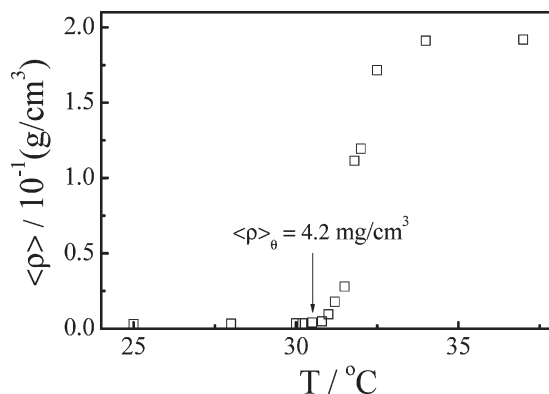


Figure 5. Solution-temperature dependent average chain density ($\langle \rho \rangle_{\text{chain}}$), defined in terms of its hydrodynamic volume, of poly(*N*-isopropylacrylamide) in water, where the arrow points to the polymer density at Θ temperature.

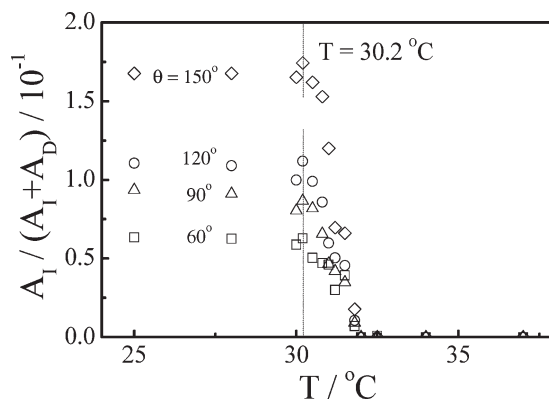


Figure 6. Solution-temperature dependent area ratio $A_I/(A_I + A_D)$ of two peaks, respectively, related to internal motions and diffusion of poly(*N*-isopropylacrylamide) linear chains in water at different scattering angles, where the dashed line marks the point at which internal motions become the strongest.

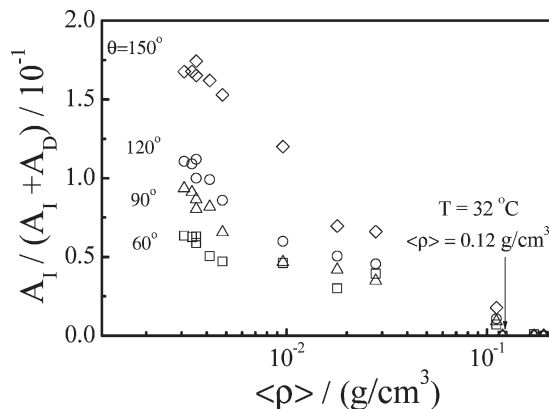


Figure 7. Average chain-density dependent area ratio $A_I/(A_I + A_D)$ of two peaks, respectively, related to internal motions and diffusion of poly(*N*-isopropylacrylamide) linear chains in water at different scattering angles, where the arrow points to the density at which internal motions are completely suppressed.

density, $A_I/(A_I + A_D)$ increases with the scattering angle. This is because at a smaller $1/q$, one probes more internal motions inside each coiled chain, especially when it is in its highly swollen state at lower temperatures. Note that $\langle \rho \rangle_{\text{chain}}$ can be read as the average local polymer concentration inside the hydrodynamic volume of each polymer chain. Therefore, Figure 7 actually reveals how the

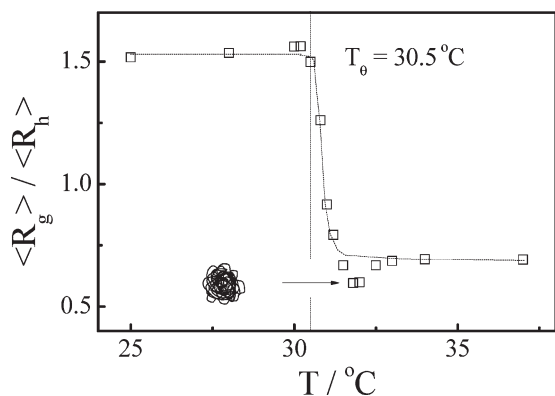


Figure 8. Solution-temperature dependent ratio of average radius of gyration and hydrodynamic radius of poly(*N*-isopropylacrylamide) linear chains in water, where the dashed line marks the Θ temperature and the arrow points to the molten globule state, which is schematically shown on the left.

chain crowding suppresses the internal motions of individual chains, reflecting in the fact that $A_I/(A_I + A_D)$ decreases as $\langle \rho \rangle_{\text{chain}}$ increases and finally approaches zero at $\langle \rho \rangle_{\text{chain}} \sim 1.2 \times 10^{-1} \text{ g/cm}^3$ that is ~ 135 times higher than its overlapping concentration in water at 25.0°C .

In order to further illustrate why the internal motions of linear PNIPAM chains disappear at higher temperatures, we plot the temperature dependence of the ratio of the average radius of gyration to the average hydrodynamic radius, as shown in Figure 8. $\langle R_g \rangle / \langle R_h \rangle$ is a parameter that describes the chain conformation. For linear flexible chains in good solvent and hard spheres with a uniform density, both theoretical and experimental studies have showed that $\langle R_g \rangle / \langle R_h \rangle \sim 1.5$ and ~ 0.77 , respectively.²³

As expected, the change of $\langle R_g \rangle / \langle R_h \rangle$ would follow the dash line in Figure 8 and approach 0.77 when the chain is fully collapsed. However, we have consistently observed a dip (minimum) of $\langle R_g \rangle / \langle R_h \rangle$ before the chain reaches its globular state. Such a dip is related to the so-called molten globular state in which many small loops are formed on the periphery of a shrunk chain,³¹ as schematically shown in Figure 8. These small loops lead to a larger hydrodynamic size but have little effect on the radius of gyration because of their insignificant masses, so that $\langle R_g \rangle / \langle R_h \rangle < 0.774$ predicted for a uniform nondraining sphere. A combination of Figures 6 and 8 clearly reveal that the internal motions are still visible when $\langle R_g \rangle / \langle R_h \rangle$ is still in the dip but disappears after it reaches the plateau, supporting our previously proposed concept of the molten globular state.

Further, we conducted a parallel study of PNIPAM spherical microgels. Figure 9 shows how they shrink with an increasing temperature. A comparison of Figures 2 and 9 shows that the microgels collapse much less than the chains, presumably due to the cross-linking that already prevents the swollen of the gel network at lower temperatures. In contrast to linear chains where internal motions were observed at $x \sim 1$, the second peak related with the internal motions of the microgels is much weak and appears only when $x \geq 8$ at 25.0°C ; namely, we can only observe their internal motions when $1/q \sim 50 \text{ nm} \leq \langle R_g \rangle / 3$, instead of at $1/q \sim \langle R_g \rangle$, implying that the thermal energy can excite the entire linear chain with its longest normal mode, but only a small portion of a gel network with a dimension of $\sim 50 \text{ nm}$.

Figure 10 shows that at 31.5°C , we start to see the internal motions at a smaller x (~ 5 – 6), which implies that the thermal energy excites a larger portion of the gel network to undergo the internal motions and the microgel becomes softer. If imaging that the gel network is made of small uniform meshes with a dimension of $\sim 10 \text{ nm}$ on the basis of the cross-linking density, we are able to estimate that the internal motions only involve about

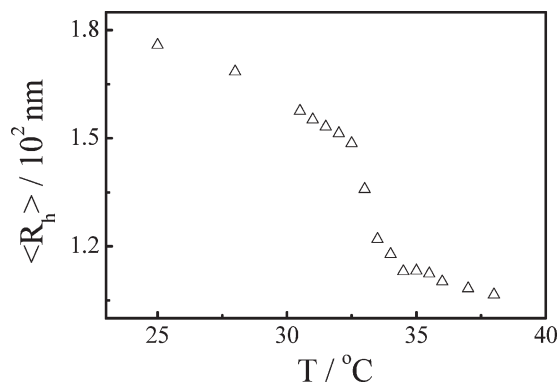


Figure 9. Dispersion-temperature-dependent average hydrodynamic radius of poly(*N*-isopropylacrylamide) spherical microgels in water.

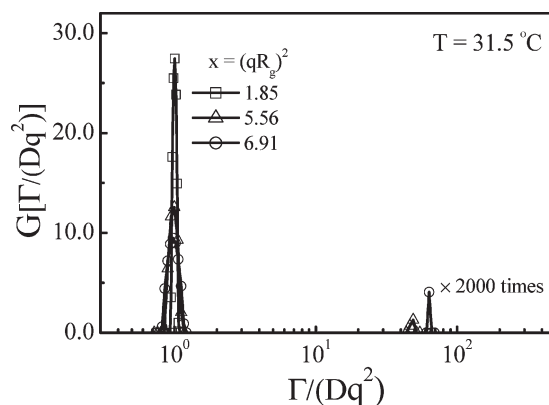


Figure 10. x -dependent q^2 -scaled line-width distributions $G[\Gamma/(Dq^2)]$ of poly(*N*-isopropylacrylamide) microgels in water, where the peak related to internal motions is enlarged by a factor of 2000 for a better view.

$\sim 10^2$ of such meshes from the minimum $1/q$. Note that such measured internal motions are slower than the relaxation of the subchains (“blobs”) of a macroscopic gel network with a similar cross-linking density, but faster than the translational diffusion of individual microgels in dispersion.

Figure 11 reveals that $A_I/(A_I + A_D)$ initially increases as the microgels shrink in the good solvent region, reflecting the increase of the average chain density with the temperature. Further increase of the temperature leads to a more and quick collapse of the microgels as well as a sharp decrease of $A_I/(A_I + A_D)$, starting at 32.5°C that is two degrees higher than the Θ temperature of PNIPAM linear chains in water. At 37°C , the microgel approaches their fully collapsed state and $A_I/(A_I + A_D)$ becomes zero, indicating complete suppression of the internal motions. The increase of $A_I/(A_I + A_D)$ can be attributed to a gradual decrease of the entropic elasticity (elastic module) of the gel network because the microgel becomes “softer” when it swells less as the dispersion approaches its Θ temperature.

Following our previous argument that a polymer chain should be mostly deformable at its ideal state; namely, the interaction among its segments is balanced by that between solvent and segment, we can mark this turning point of $A_I/(A_I + A_D)$ as the Θ temperature of the PNIPAM microgels in water. It has been known that the volume phase transition of a gel network, depending on whether it has a lower or upper critical solution temperature (LCST or UCST), shifts to a higher or lower temperature as the cross-linking density increases, i.e., the average length of the subchains between two neighboring cross-linking points decreases.³⁴ For a PNIPAM gel network in water with a LCST, the shift of its Θ temperature from 30.5 to 32.5°C is

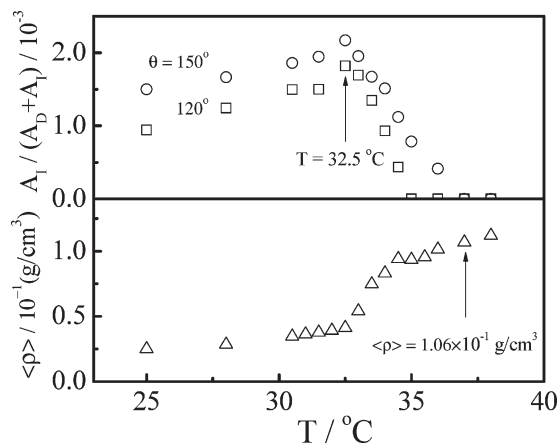


Figure 11. Dispersion-temperature dependent average chain density ($\langle \rho \rangle_{\text{chain}}$) defined in terms of its hydrodynamic volume, and area ratio $A_I/(A_I + A_D)$ of two peaks, respectively, related to internal motions and diffusion of poly(*N*-isopropylacrylamide) spherical microgels in water at two different scattering angles, where dash line marks the temperature at which internal motions become the strongest and the arrow points to the density when internal motions are completely suppressed.

reasonable.²⁴ To further test the validity of using the temperature dependent area ratio of the two peaks in the measured line-width distribution to estimate the Θ condition, we also studied a well accepted system, polystyrene in cyclohexane, and found that the area ratio makes the turning point at ~ 35.0 °C (not shown), slightly higher than ~ 34.5 °C that is the widely accepted value in literature. Such a small difference might be attributed to the difference between the ideal state of a single chain and ideal state of polymer solution.

For a single chain in a solution, its unperturbed “ideal” state reflects the condition at which the entropic cost due to the chain swelling caused by the excluded volume balances the segment–segment or segment–solvent interaction; while for a dilute polymer solution, the existence of more than one chains in solution leads to additional interchain interaction that only vanishes at infinite dilution. Practically, we normally determine the Θ -condition of a polymer solution from $A_2 = 0$, not the unperturbed state of a single chain.

It should be noted that the Θ conditions (temperature or solvent composition) of many polymer solutions were previously determined and tabled in polymer handbooks by using static and interchain interaction-related properties measured by various methods, including static LLS, osmotic pressure and viscosity. However, some of these Θ conditions measured by different methods or reported by different groups significantly vary in a wide range even for an identical polymer/solvent system.³⁵ For example, for poly(ethylene oxide) in water and poly(methyl methacrylate) in acetonitrile, the Θ temperature, respectively, varies from 80 to 113 °C and from 32 to 45 °C and is not correlated to the chain length as predicted. The uncertainty is partially due to natures of these experimental methods. There is also some uncertainty of using our observed turning point as the Θ temperature of a single chain in solution but it is estimated to be no more than ± 0.5 °C. More importantly, such a turning point in the relative intensity contribution of the internal motions is an *intrachain and dynamic* property and closer to the definition of the unperturbed state of a single chain in solution. More theoretical studies are needed to quantitatively understand this turning point.

Conclusion

A comparison of internal motions of poly(*N*-isopropylacrylamide) linear chains and spherical microgels in the Θ and poor

solvents reveals that the thermal energy ($k_B T$) is able to excite the entire linear chain to undergo the longest normal mode, but only a portion of the microgel network with a dimension of ~ 50 nm, on the basis of the lowest scattering vector (q) at which the internal motions appear in the characteristic line-width distribution measured in dynamic laser light scattering. Namely, the internal motions of linear chains and spherical microgels at the room temperature are detectable only when $x \geq 1$ and 8, respectively, where $x = (qR_g)^2$ with R_g the radius of gyration. We also found that the contribution of internal motions makes a turning point around Θ temperature, presumably because the chain becomes the most deformable (the softest) when the interaction among chain segments and among solvent molecules and segments are balanced. Such a finding leads to a convenient way to estimate the Θ condition of a given polymer solution. Further, our results reveal that the internal motions are gradually suppressed during the coil-to-globule transition of individual linear chains or subchains inside the microgel network when the solvent quality changes from good to poor, implying that the internal motions should be suppressed when the chains are overlapped in the semi- and concentrated regions.

Acknowledgment. The financial support of Ministry of Science and Technology of China (2007CB936401), the National Natural Scientific Foundation of China (NNSFC) Projects (20934005 and 50773077) and the Hong Kong Special Administration Region Earmarked Project (CUHK4039/08P, 2160361) is gratefully acknowledged.

Supporting Information Available: Figures showing plots of temperature dependent normalized scattering intensities and relative contribution of internal motions. This material is available free of charge via the Internet at <http://pubs.acs.org>.

References and Notes

- (1) Rouse, P. E. *J. Chem. Phys.* **1953**, *21*, 1271.
- (2) Zimm, B. H. *J. Chem. Phys.* **1956**, *24*, 269.
- (3) Pecora, R. *J. Chem. Phys.* **1968**, *49*, 1032.
- (4) de Gennes, P.-G. *Physics* **1967**, *3*, 37.
- (5) Han, C. C.; Akcasu, A. Z. *Macromolecules* **1981**, *14*, 1080.
- (6) Chu, B. *J. Polym. Sci., Polym. Symp.* **1985**, *73*, 137.
- (7) Dubois-Violette, E.; de Gennes, P. -G. *Physics* **1967**, *3*, 181.
- (8) Kramer, O.; Frederick, J. E. *Macromolecules* **1972**, *5*, 69.
- (9) McAdam, J. D.G.; Knox, A.; King, T. A. *Chem. Phys. Lett.* **1973**, *19*, 351.
- (10) McAdam, J. D.G.; King, T. A. *Chem. Phys.* **1974**, *6*, 109.
- (11) Nicolai, T.; Brown, W.; Johnsen, R. M. *Macromolecules* **1989**, *22*, 2795.
- (12) Pecora, R. *J. Chem. Phys.* **1965**, *43*, 1762.
- (13) Perico, A.; Piaggio, P.; Cuniberti, C. *J. Chem. Phys.* **1975**, *62*, 2690. Perico, A.; Piaggio, P.; Cuniberti, C. *J. Chem. Phys.* **1975**, *62*, 4911.
- (14) Tsunashima, Y.; Hirata, M.; Nemoto, N.; Kurata, M. *Macromolecules* **1983**, *16*, 584.
- (15) Nemoto, N.; Makita, Y.; Tsunashima, Y.; Kurata, M. *Macromolecules* **1984**, *17*, 425.
- (16) Brown, W.; Johnsen, R.; Stepanek, P.; Jakes, J. *Macromolecules* **1988**, *21*, 2859.
- (17) Bhatt, M.; Jamieson, A. M. *Macromolecules* **1988**, *21*, 3015.
- (18) Bhatt, M.; Jamieson, A. M. *Macromolecules* **1989**, *22*, 2724.
- (19) Chu, B.; Wang, Z. L.; Yu, J. Q. *Macromolecules* **1991**, *24*, 6832.
- (20) Sawatari, N.; Yoshizaki, T.; Yamakawa, H. *Macromolecules* **1998**, *31*, 4218.
- (21) Yoshida, N.; Yoshizaki, T.; Yamakawa, H. *Macromolecules* **2000**, *33*, 3254.
- (22) Zhou, S. Q.; Wu, C. *Macromolecules* **1996**, *29*, 1574.
- (23) Wang, X. H.; Wu, C. *Phys. Rev. Lett.* **1998**, *80*, 4092.
- (24) Senff, H.; Richtering, W. *J. Chem. Phys.* **1999**, *111*, 1705.
- (25) Zhou, S. Q.; Fan, S. Y.; Au-yeung, S. T. F.; Wu, C. *Polymer* **1995**, *36*, 1341.
- (26) Zhou, S. Q.; Wu, C. *J. Macromol. Sci. Phys.* **1997**, *B36*, 345.
- (27) Chu, B. *Laser Light Scattering*, 2nd ed.; Academic Press: New York, 1991.
- (28) Berne, B.; Pecora, R. *Dynamic Light Scattering*; Plenum Press: New York, 1976.

- (29) Provencher, S. W. *Biophys. J.* **1976**, *16*, 29. *J. Chem. Phys.* **1976**, *64*, 2772; *Makromol. Chem.* **1979**, *180*, 201.
- (30) Teraoka, I. *Polymer solution*; John Wiley Sons: Inc.: New York, 2002.
- (31) Zhou, S. Q.; Wu, C. *Phys. Rev. Lett.* **1996**, *77*, 3053.
- (32) Sorlie, S. S.; Pecora, R. *Macromolecules* **1988**, *21*, 1437.
- (33) Zimm, B. H.; Roe, G. M. *J. Chem. Phys.* **1956**, *24*, 279.
- (34) Dušek, K.; Patterson, D. *J. Polym. Sci. Part A-2* **1968**, *6*, 1209.
- (35) Brandrup, J.; Immergut, E. H.; Grulke, E. A., Ed. *Polymer Handbook*; Wiley: New York, 1999.